Hydrol. Earth Syst. Sci. Discuss., 9, 895–936, 2012
www.hydrol-earth-syst-sci-discuss.net/9/895/2012/
doi:10.5194/hessd-9-895-2012
© Author(s) 2012. CC Attribution 3.0 License.

Hydrology and Earth System Sciences Discussions

This discussion paper is/has been under review for the journal Hydrology and Earth System Sciences (HESS). Please refer to the corresponding final paper in HESS if available.

Spatial and temporal variability of biophysical variables in Southwestern France from airborne L-band radiometry

E. Zakharova[1], J.-C. Calvet[1], S. Lafont[1], C. Albergel[1,*], J.-P. Wigneron[2], M. Pardé[3], Y. Kerr[4], and M. Zribi[4]

[1]CNRM-GAME, Météo-France, CNRS, URA1357, 42 avenue Gaspard Coriolis, Toulouse, France
[2]INRA, EPHYSE, 71 avenue Edouard Bourlaux, Villenave d'Ornon, France
[3]LATMOS/CNRS, Route de Troux, 78280 Guyancourt, France
[4]CESBIO, CNES/CNRS/IRD/UPS, UMR5126, 18 Avenue Edouard Belin, Toulouse, France
[*]now at: ECMWF, Shinfield Park, Reading, UK

Received: 5 January 2012 – Accepted: 10 January 2012 – Published: 17 January 2012

Correspondence to: J.-C. Calvet (jean-christophe.calvet@meteo.fr)

Published by Copernicus Publications on behalf of the European Geosciences Union.

Abstract

In 2009 and 2010 the L-band microwave Cooperative Airborne Radiometer for Ocean and Land Studies (CAROLS) campaign was performed in Southwestern France to support the calibration and validation of the new Soil Moisture and Ocean Salinity (SMOS) satellite mission. The L-band Microwave Emission of the Biosphere (L-MEB) model was used to retrieve Surface Soil Moisture (SSM) and the Vegetation Optical Depth (VOD) from the CAROLS brightness temperature measurements. The CAROLS SSM was compared with in situ observations at 11 sites of the SMOSMANIA (Soil Moisture Observing System-Meteorological Automatic Network Integrated Application) network of Météo-France. For eight of them, significant correlations were observed ($0.51 \leq r \leq 0.82$), with standard deviation of differences ranging from $0.039\,m^3\,m^{-3}$ to $0.141\,m^3\,m^{-3}$. Also, the CAROLS SSM was compared with SSM values simulated by the A-gs version of the Interactions between Soil, Biosphere and Atmosphere (ISBA-A-gs) model along twenty flight lines, at a resolution of 8 km × 8 km. A significant spatial correlation between these two datasets was observed for all the flights ($0.36 \leq r \leq 0.85$). The CAROLS VOD presented significant spatial correlations with the vegetation water content (VWC) derived from the spatial distribution of vegetation types used in ISBA-A-gs and from the Leaf Area Index (LAI) simulated for low vegetation. On the other hand, the CAROLS VOD presented little temporal changes, and no temporal correlation was observed with the simulated LAI. For low vegetation, the ratio of VOD to VWC tended to decrease, from springtime to summertime. For 83 % of ISBA-A-gs grid cells (8 km × 8 km), sampled every 5 m by CAROLS observations at a spatial resolution of about 2 km, the standard deviation of the sub-grid CAROLS SSM was lower than $0.05\,m^3\,m^{-3}$. The presence of small water bodies within the ISBA-A-gs grid cells tended to increase the CAROLS SSM spatial variability, up to $0.10\,m^3\,m^{-3}$. Also, the grid cells characterised by a high vegetation cover heterogeneity presented higher standard deviation values, for both SSM and VOD.

HESSD

9, 895–936, 2012

1 Introduction

Biophysical variables such as soil moisture, Leaf Area Index (LAI), and vegetation biomass, need to be monitored for applications in ecohydrology, hydrometeorology and agroclimatology, at global and regional scales. Soil moisture plays an important role in hydrological models, controlling the soil drainage and the surface runoff. It is also a crucial variable for Land Surface Models (LSM), as it regulates the water and energy surface fluxes. Finally, the seasonal dynamics of vegetation properties, such as LAI, is connected to soil moisture dynamics (Kochendorfer and Ramirez, 2010). Developing observation capacities able to monitor the spatial and temporal variability of vegetation and soil moisture characteristics at a regional scale is needed for eco-hydrology research. This remote sensing study investigates the joint temporal and spatial soil moisture dynamics and vegetation growth as observed at the regional scale by the airborne Cooperative Airborne Radiometer for Ocean and Land Studies (CAROLS) L-band radiometer. The analysis is based on a very high number of flights (20 flights covering the same transect), in situ soil moisture observations, and simulated biophysical variables.

The satellite-derived surface soil moisture (SSM) or soil wetness index (SWI) products from passive (e.g. the Advanced Microwave Scanning radiometer on EOS – AMSR-E) and active (the Advanced Scatterometer – ASCAT, and the European Remote Sensing Satellite Scatterometer – ERS-Scat) C-band microwave sensors were recently validated over Southwestern France (Albergel et al., 2009; Pellarin et al., 2006; Rüdiger et al., 2009), Western Africa (Gruhier et al., 2010; De Rosnay et al., 2009), Canada and Ukraine (Wagner et al., 1999a,b), China (Zhao et al., 2008), the United States of America (Drusch et al., 2004) and Australia (Draper et al., 2007). Passive sensors operating in the low frequencies microwave range (1–10 GHz) are of particular interest as with decreasing frequency the thickness of the sampled soil layer increases, the vegetation masking effect on SSM tends to decrease, and atmospheric effects are weaker (Wagner et al., 2007).

HESSD
9, 895–936, 2012

The high capability of SSM retrieval at L-band (1–2 GHz) was demonstrated by several studies (e.g., Wigneron et al., 2002; Kerr et al., 2001; De Rosnay et al., 2006; Calvet et al., 2011). The first ground-based studies dedicated to soil moisture measurement at L-band started in the 1980s (Jackson et al., 1986). Later, they were complemented by airborne measurements (Jackson et al., 1986; Schmugge et al., 1992; Chanzy et al., 1997), that finally led to the development the SMOS (Soil Moisture and Ocean Salinity) spaceborne instrument operating at L-band (Kerr et al., 2001). The SMOS SSM retrieval algorithm is based on the inversion of the L-band Microwave Emission of the Biosphere model (L-MEB), which simulates the L-band emission of the soil-plant system (Wigneron et al., 2007).

A number of field experiments (CoSMOS, SMOSREX, VAS, MELBEX-1, BARC, ELBARA-ETH) (Saleh et al., 2007, 2009; Cano et al., 2010) were carried out in order to prepare the SMOS mission and validate the SSM retrieval algorithm. In addition, several airborne campaigns were performed to assess SSM retrieval over large areas: EuroSTARRS in France and Spain (Saleh et al., 2004), NAFE/CoSMOS in Australia (Panciera et al., 2008), EAGLE2006 in Germany (Su et al., 2009), HOBE in Denmark (Bircher et al., 2011). The L-MEB SSM retrieval capability was extensively tested in homogeneous vegetation cover conditions (Grant et al., 2007; Saleh et al., 2007; Wigneron et al., 2007; Guglielmetti et al., 2008), and over a heterogeneous 40 km × 40 km SMOS pixel in Australia in the framework of the NAFE airborne experiment (Panciera et al., 2008). However, there is still a need to assess the accuracy of SSM retrievals for various ground properties and vegetation types. Besides SSM, the retrieval algorithm based on L-MEB produces a L-band vegetation optical depth (VOD). The VOD values depend on the considered microwave frequency, are sensitive to the vegetation canopy properties and are related to the vegetation water content (VWC) (Wigneron et al., 1995). The latter is of interest to monitor agricultural droughts (Penuelas et al., 1993) and the forest fire risk (Davidson et al., 2006). Also, it is an important parameter for the estimation of the surface albedo (Wang et al., 2005). Jones et al. (2011) demonstrated that the VOD retrieved from AMSR-E, operating at C-band,

HESSD
9, 895–936, 2012

correlates with MODIS satellite-derived vegetation metrics such as LAI. The capability of L-band derived VOD to represent the vegetation variability over large heterogeneous regions is still unclear.

One of the more recent airborne campaigns dedicated to SMOS is the CAROLS experiment, co-funded by CNES and ESA. CAROLS was performed in 2009 and 2010 in Southwestern France and in Spain (Zribi et al., 2011; Pardé et al., 2011a). Albergel et al. (2011) showed the good sensitivity of the CAROLS L-band brightness temperatures (Tb) to the SSM variability at 11 stations of the SMOSMANIA soil moisture network (Calvet et al., 2007; Albergel et al., 2008), with an average correlation coefficient of −0.76 at nadir. However, Radio-Frequency Interferences (RFI) affected the CAROLS observations (Albergel et al., 2011; Pardé et al., 2011a; Zribi et al., 2011).

In this study, the temporal and spatial variability of the SSM and VOD values retrieved by L-MEB from 2009 and 2010 springtime CAROLS Tb observations in Southwestern France is investigated. Details on the parameterisation of the L-MEB model are given in Pardé et al. (2011b). In a first stage, post-processing techniques are used to limit the detrimental impact on the retrievals of RFI and open water surfaces. Then, the accuracy of the SSM retrievals is assessed using in situ SSM observations at eleven instrumented sites. The CAROLS SSM and VOD transects are compared with SSM and Leaf Area Index (LAI) simulations of the CO_2-responsive version of the Interactions between Soil, Biosphere and Atmosphere (ISBA-A-gs) model, over 8 km×8 km grid-cells.

HESSD
9, 895–936, 2012

2 Data and methods

2.1 The CAROLS data

2.1.1 The CAROLS instrument

The CAROLS L-band microwave radiometer is fully polarimetric and has two antennas, one looking at nadir and a side-looking antenna slanting with an incidence angle of 33.5°. The sampling frequency range is 1401–1426 MHz and an advanced analogue filter permits the suppression of the main RFI affecting the Tb. The instrument sensitivity is 0.1 K for 1s integration time and the stability is better than 0.1 K over 15 min. The internal calibration is achieved by load and noise diodes. The radiometer was calibrated during test flights performed in November 2008 (Zribi et al., 2011).

2.1.2 The 2009 and 2010 flights in Southwestern France

The CAROLS microwave Tb airborne measurements were carried out from the French ATR-42 research aircraft, together with infrared temperature (T_{IR}) observations performed by a CIMEL radiometer. The flights consisted of straight lines between Toulouse and the Atlantic coast (Bay of Biscay), then to the Mediterranean coast, and back to Toulouse (Fig. 1). They were performed at an altitude of 2000 m a.s.l., and the ground footprint sizes of the nadir and side looking antennas were about 1.4 km and 2.1 km, respectively (Albergel et al., 2011). The along track spatial resolution was about 5 m. The transect between the Bay of Biscay and the Mediterranean Sea was about 385 km, and the complete flights were covered in 3 h.

In 2009, six CAROLS flights were conducted over Southwestern France between 28 April and 27 May and all of them are used in this study. While half of them (28 April, 15 and 27 May) covered the whole transect, the others (18, 20 and 26 May) covered the Toulouse-Atlantic coast transect (225 km long), only. Fourteen flights performed in 2010, covering the full transect between 15 April and 1 July, are used in this study.

HESSD
9, 895–936, 2012

The flights were performed in the morning (between 05:00 UTC and 08:00 UTC), apart from four of them (18 and 27 May 2009, 4 and 22 June 2010), performed in the late afternoon (between 18:00 UTC and 20:00 UTC).

The flights did not cover mountainous areas and the surface altitude varied between 0 m a.s.l. and 400 m a.s.l. The transect can be divided into three main areas:

- the Atlantic lowland plain, between 1° W and 0.2° W, corresponding to the Les Landes pine forest, on sandy soils (with sand fractions of about 90 %)
- the hilly Armagnac, Garonne terraces and Lauragais regions, corresponding to undulating terrain, intersected by numerous rivers, and mainly covered by croplands (e.g. wheat and irrigated maize), by grassland and forest patches over the steepest slopes, and with areas covered by vineyards, on loamy soils with clay and sand fractions varying between 20 % and 30 %. This part of the transect presents the highest altitudes (from 150 m to 380 m). The soils are characterised by a higher clay content (20–30 %), in comparison with the surrounding regions.
- the Mediterranean plain, between 2.1° E and 3.3° E is flat and the vegetation cover is contrasted, with forest patches alternating with sparse vegetation, dry shrubs, and vineyards. In the easternmost part the soils are more sandy, with sand fractions ranging from 40 % to 50 %.

2.1.3 SSM and VOD retrievals

The SSM and VOD values were retrieved from the biangular/dual-polarized L-band CAROLS Tb measurements, inverting the most recent version of the L-MEB model (Panciera et al., 2008; Pardé et al., 2011a,b). As, according to the Fresnel law, TbV and TbH values are confounded at nadir, only three independent Tb values are used in the inversion: Tb at nadir, and slant (33.5°) TbV and TbH. The present version uses the Dobson model (Dobson et al., 1985) of the soil microwave dielectric properties. The soil roughness is accounted for using the Wang and Choudhury (1981) model, based

HESSD
9, 895–936, 2012

on two parameters, h and Q. The Q parameter is set to zero and the h parameter is related to SSM as proposed by Saleh et al. (2007) for a grassland site in Southwestern France, and applied by Pardé et al. (2011b) to the CAROLS data:

$$h = 1.3 - 1.13 \times \mathrm{SSM} \quad (1)$$

with SSM in units of $m^3\,m^{-3}$.

The vegetation contribution is computed using the τ-ω approach, where τ represents VOD, and ω represents the single scattering albedo of the vegetation, assumed to be close to zero. The effective temperature (T_{eff}) contribution is approximated as:

$$T_{\mathrm{eff}} = T_{\mathrm{depth}} + (T_{\mathrm{IR}} - T_{\mathrm{depth}}) \times (\mathrm{SSM}/w)^{\beta} \quad (2)$$

where T_{depth} is the ground temperature at a depth of 30 cm measured at the meteorological stations of the SMOSMANIA network (see Sect. 2.2) and then interpolated along the aircraft transect, and T_{IR} is the infrared temperature, remotely sensed from the aircraft. The w and β parameters have constant values: $0.30\,m^3\,m^{-3}$ and 0.3, respectively (Grant et al., 2008; Wigneron et al., 2007). The soil properties like the sand and clay contents used in the model are derived from the SMOSMANIA auxiliary dataset (Albergel et al., 2008) linearly interpolated along the CAROLS flight transect.

2.1.4 Mitigation of perturbing factors

In Southwestern France the CAROLS microwave measurements are affected by Radio-Frequency Interference (RFI) and by the presence of water bodies. Albergel et al. (2011) had to filter out about half of CAROLS Tb observations affected by RFI, over 11 SMOSMANIA sites. The RFI tend to increase the Tb values and undetected RFI may result in the underestimation of SSM and/or in the overestimation of VOD. The structure and quality of the CAROLS observations, as well as the RFI sources and their detection were described in detail by Pardé et al. (2011a) and Zribi et al. (2011). Before applying the SSM and VOD retrieval algorithm, a method of detection and mitigation of

HESSD
9, 895–936, 2012

the undesirable effects of RFI was applied to the CAROLS Tb dataset by Pardé et al. (2011a). The analysis of the SSM and VOD products performed in this study showed that further RFI filtering is needed.

As illustrated by Fig. 2, a number of unrealistic SSM values, close to 1 $m^3 m^{-3}$ or higher than 1 $m^3 m^{-3}$, as well as a lot of smaller peaks are obtained. The spatial analysis of the successful SSM retrievals shows that the perturbation of SSM values are obtained over areas where (1) very low Tb values and/or (2) significant differences between nadir V- and H-polarized Tb are observed (TbV and TbH, respectively). In order to improve the retrievals, a post-processing filtering technique was applied to the data set. This method is based on the paired view analysis of TbV and TbH at nadir. According to the Fresnel law, at nadir the surface emissivities at vertical and horizontal polarizations are equal. Therefore, the difference between nadir TbH and nadir TbV (Δ Tb) should not depart much from zero. It was assumed that all the retrievals corresponding to Δ Tb values higher or lower than $\pm$ two standard deviations (calculated using all 20 flights) were affected by RFI. Filtering the data using this criterion removed many peaks around the largest urban areas.

A second filtering criterion was based on the analysis of TbH vs. TbV at 33.5° for the 2009 flights (Fig. 3). A density-based clustering method was applied to contour a main cluster A (Fig. 3), and remove the data outside this cluster. The detection of the cluster borders depends on a density threshold, which was determined using the 2009 data, in order to optimize the spatial correlation between the retrieved and the modelled SSM values. The same threshold was used for the 2010 data. The spatial analysis of the outliers corresponding to high TbH and to high TbV values (B and C subsets of Fig. 3, respectively) indicates that they are caused by unmitigated RFI perturbations close to urban areas (not shown). The D cluster corresponds to low values of both TbH and TbV, observed in regions presenting a high density of water bodies (not shown). In order to further reduce the impact of open water surfaces, we have arbitrarily excluded the cluster A measurements corresponding to TbH values less than 220 K. It removed all the unrealistic SSM higher than 1 $m^3 m^{-3}$ (Fig. 2). The

HESSD
9, 895–936, 2012

application of the above-mentioned post-processing filtering techniques permitted to improve significantly the overall quality of the SSM and VOD retrieval data set.

2.2 SMOSMANIA stations

The SSM retrievals were validated using in situ observations of the Soil Moisture Observing System – Meteorological Automatic Network Integrated Application (SMOSMANIA) network (Calvet et al., 2007). This network consists of 12 stations operating since January 2007. It is based on the existing automatic weather station network of Météo-France, and standard hydrometeorological observations (precipitation, air temperature, air humidity, wind speed) are measured, also. The stations form a transect between the Atlantic coast and the Mediterranean sea (Fig. 1) and sample soil moisture under contrasting climatic conditions (Albergel et al., 2008). At each station, the soil moisture acquisition is done every 12 min by four ThetaProbe ML2X instruments at 5 cm, 10 cm, 20 cm and 30 cm depths. Soil temperature is measured at the same depths. The soil moisture dataset is available online at http://www.ipf.tuwien.ac.at/insitu/. The observations from this network were extensively used for the validation of modelled and satellite-derived soil moisture (Albergel et al., 2008, 2009, 2010, 2011; Parrens et al., 2012).

2.3 ISBA-A-gs surface soil moisture and LAI simulations

In order to assess the ability of the CAROLS measurements to represent the spatial and temporal variability of SSM and VOD, the retrievals were compared with SSM and LAI simulations produced by the ISBA-A-gs LSM, at a spatial resolution of 8 km × 8 km. Prior to the comparison, the airborne observations were averaged within each ISBA-A-gs grid cell crossed by the flight line. As Tb values are very sensitive to open water surfaces, the grid cells with water fraction more than 0.8 % (corresponding to a total open water area of 0.5 km^2) were removed.

HESSD
9, 895–936, 2012

The SSM and LAI simulations were made using the SURFEX (SURFace EXternalisée) platform developed at Météo-France. ISBA-A-gs is a version of the ISBA LSM that includes a photosynthesis and a plant growth model (Calvet et al., 1998, 2004; Calvet, 2000; Calvet and Soussana, 2001). The simulations were driven by the SAFRAN analysis of surface meteorological variables (Durand et al., 1993; Quintana-Segui et al., 2008) and the spatial distribution of the model parameters was based on ECOCLIMAP-II (Masson et al., 2003; Faroux et al., 2009).

The ISBA-A-gs version used in this study simulates three soil layers. The simulated SSM corresponds to the modelled surface soil layer, about 1 cm thick. The sub-grid heterogeneity is represented by aggregating the simulations performed for the various surface types found in the grid cell, according to the surface type fractions provided by ECOCLIMAP-II (Brut et al., 2009). Also, this allows to provide separate estimates of SSM and LAI for high (trees) and low (grasslands and crops) vegetation types.

The LAI simulations of ISBA-A-gs can be used, to some extent, to estimate the VWC affecting the L-band land emission. In a study at a global scale, Pellarin et al. (2003) assumed that the VWC of low vegetation (grasslands and crops) could be estimated, as $0.5\times$ LAI, in units of $\mathrm{kg\,m^{-2}}$. For forest canopies they set constant values of VWC, as at L-band this quantity depends mostly on the water content of the branches. The latter was estimated by Pellarin et al. (2003) as $3\,\mathrm{kg\,m^{-2}}$ and $4\,\mathrm{kg\,m^{-2}}$ for coniferous and deciduous trees, respectively. As lower branch water content values were reported by Grant et al. (2008) for European forests, the values $1.5\,\mathrm{kg\,m^{-2}}$ and $3\,\mathrm{kg\,m^{-2}}$ are used in this study, for coniferous and deciduous trees, respectively. Using the LAI simulated by ISBA-A-gs, the vegetation water content affecting the L-band land emission for low (grasslands and crops) and high (forests) vegetation, $\mathrm{VWC_{low}}$ and $\mathrm{VWC_{high}}$, respectively, are estimated along the aircraft transect as (in units of $\mathrm{kg\,m^{-2}}$):

$$\mathrm{VWC_{low}} = 0.5 \times \mathrm{LAI_{low}} \quad (3a)$$

$$\mathrm{VWC_{high}} = 1.5 \times \alpha_{\mathrm{conif}} + 3 \times \alpha_{\mathrm{decid}} \quad (3b)$$

HESSD
9, 895–936, 2012

where LAI_{low} is the LAI of low vegetation in a given grid cell, and α_{conif} and α_{decid} are coniferous and deciduous forest fractions, respectively. Finally, VOD can be derived from VWC as:

$$VOD_{low} = b_{low} VWC_{low} \quad (4c)$$

$$VOD_{high} = b_{high} VWC_{high} \quad (4d)$$

where b_{low} and b_{high} are constant values, for a given vegetation type. Pellarin et al. (2003) proposed b_{low} values ranging from 0.15 to 0.20 $m^2\,kg^{-1}$ for low vegetation (crops and grasslands, respectively), and $b_{high} = 0.33\,m^2\,kg^{-1}$. Grant et al. (2008) found a b_{high} value of $0.4\,m^2\,kg^{-1}$ for 26-yr old pine trees. Also, values of b_{high} and b_{low} can be obtained by inverting Eq. (4) for the flights presenting a significant spatial correlation between VWC and VOD, with VWC and VOD estimates derived from ISBA-A-gs and from CAROLS, respectively, for grid-cells with a fraction of woody vegetation higher than 70 %, and with a fraction of low vegetation higher than 80 %, respectively (see Sect. 3.2.2). Using these average values of b_{high} and b_{low}, aggregated bottom-up VOD values can be calculated from the ISBA-A-gs model for each flight: the VWC and VOD values derived from Eqs. (3)–(4) for low and for high vegetation are aggregated over each ISBA-A-gs grid-cell using a linear mixing equation based on the ECOCLIMAP-II vegetation fractions.

2.4 Investigating the ISBA-A-gs sub-grid variability using the CAROLS retrievals

While the ground footprint of the CAROLS radiometer is about 1.4 km at nadir, its along track spatial resolution allows sampling Tb every 5 m. Each ISBA-A-gs grid cell (8 km × 8 km) may contain up to about 500 CAROLS retrievals. After the pre- and post-processing filtering, about 60 valid SSM and VOD retrievals are obtained, on average. This over-sampling capability was used to investigate the sub-grid variability of the model's parameters in grid-cells.

HESSD
9, 895–936, 2012

2.5 Satellite LAI product

In this study, the Collection 5 version of the MODIS LAI product was used to compare the temporal evolution of the CAROLS-derived VOD with another vegetation parameter obtained by remote sensing. The MODIS LAI retrieval consists of a main procedure that exploits the spectral information content of the MODIS surface reflectances at up to 7 spectral bands. It is based on the comparison of the daily surface reflectance retrievals with radiative transfer model entries stored in a look-up table (Knyazikhin et al., 1998). The algorithm requires a land cover classification. Therefore it has interfaces with the MODIS Surface Reflectance Product (MODAGAGG) and the MODIS Land Cover Product (MOD12Q1). A look-up table compares observed and modelled reflectances for a suite of canopy structures and soil patterns that represents an expected range of typical conditions for a given biome type (Myneni et al., 2003). The initial 10-day, 1 × 1 km MODIS LAI product was resampled to the SAFRAN 8 × 8 km spatial resolution. As the available product covered the 2000–2008 period, monthly average LAI values were calculated for each grid cell, and then compared with the CAROLS VOD retrieved for the corresponding months in 2009 and in 2010.

3 Results

3.1 CAROLS SSM validation at the SMOSMANIA stations

In order to evaluate the accuracy of the airborne L-band SSM retrievals, the latter were compared with in situ soil moisture observations performed at a depth of 5 cm at the twelve SMOSMANIA stations located in Southwestern France (Fig. 4 and Table 1). It must be noted that the Lézignan-Corbières station (LZC) did not provide SSM observations during the airborne campaign of 2010. Therefore, eleven stations are considered, only. For this comparison, the SSM retrievals were averaged over a 10 km radius zone around each station. A good correlation between airborne and in situ observations is

HESSD
9, 895–936, 2012

found for 8 over 11 stations. For the three other stations, Sabres (SBR), Peyrusse-Grande (PRG) and Condom (CDM), discrepancies are observed and the correlation of the CAROLS SSM retrievals with ground observations is not significant (Table 1). More often than not, at PRG and CDM stations, the CAROLS SSM retrievals are lower than the in situ data (Fig. 4). However, PRG presents one SSM retrieval much higher than the in situ observations, and the mean bias is slightly negative, in conjunction with a high Standard Deviation of Differences (SDD) value of $0.18\,m^3\,m^{-3}$.

The most marked CAROLS biases ($0.19\,m^3\,m^{-3}$ and $-0.16\,m^3\,m^{-3}$) vs. in situ observations are observed for the Urgons (URG) and Savenes (SVN) stations. As both stations are far from the CAROLS flight transect, it is likely that the station soil properties differ from those seen by the L-band radiometer. This explanation does not hold for the Montaut (MNT) station, which presents a marked bias ($0.12\,m^3\,m^{-3}$) while lying very close to the CAROLS transect. Moreover, the best correlation ($r = 0.82$) is obtained for this station. The MNT station is located in a hilly area, and while the SSM in situ measurements at this station represent well the SSM temporal variability of the area, topographical effects impact the spatial variability of SSM.

In Table 1, the CAROLS SSM retrievals are compared, also, with the ISBA-A-gs SSM simulations at the 8 km × 8 km grid cells covering the SMOSMANIA stations. For the sake of comparison, the latter are compared with the in situ observations. CAROLS presents fair correlations with ISBA-A-gs for all the stations. While, for the eastern stations (MNT, SFL, MTM, NBN), the CAROLS SSM correlates better with the in situ observations than ISBA-A-gs, systematically higher SDD values are obtained with CAROLS. On average, the CAROLS SDD scores are higher than $0.08\,m^3\,m^{-3}$. The ISBA-A-gs SSM is closer to the in situ observations, with SDD = $0.052\,m^3\,m^{-3}$, on average.

HESSD
9, 895–936, 2012

3.2 Observed and modelled spatial and temporal variability of biophysical variables along the CAROLS transect

The ISBA-A-gs LSM simulates SSM, together with the root-zone soil moisture, as prognostic variables. Also, the vegetation growth component of the model permits to simulate LAI. The simulated SSM and LAI are expected to correlate with the SSM and VOD values retrieved from the CAROLS Tb, both temporally and spatially. Figure 5 presents the SSM and LAI time series simulated by ISBA-A-gs, together with the precipitation provided by SAFRAN, over the Atlantic-Mediterranean transect of Fig. 1, for a period of 1.5 year, from the start of the CAROLS campaign in April 2009 to the end of the campaign in July 2010. The three regions described in Sect. 2.1.2 can be distinguished in both SSM and LAI time series. Higher SSM values are simulated for the central part of the transect (Armagnac, Garonne, Lauragais), in relation to a higher soil water holding capacity. Higher LAI values are simulated over the evergreen Les Landes pine forest, at the western part of the transect (3.5 $m^2\,m^{-2}$ in April, at the beginning of the 2009 and 2010 CAROLS campaigns, and up to 4.8 $m^2\,m^{-2}$ and 5.5 $m^2\,m^{-2}$ at the end of May 2009 and June 2010, respectively). In the central and eastern parts of the transect, LAI varies between 1.1 $m^2\,m^{-2}$ and 4 $m^2\,m^{-2}$, from the beginning to the end of the 2009 and 2010 CAROLS campaigns. The simulated leaf onset varies from the end of February in the Les Landes forest to the end of March in other areas. For all the transect, the maximum LAI is reached at about the end of June, i.e. at the end of the 2010 CAROLS campaigns.

3.2.1 Surface soil moisture

The various CAROLS flights permitted to sample a large range of SSM conditions, as illustrated by the SSM values simulated by ISBA-A-gs in Fig. 5. The first CAROLS flight on 28 April 2009 took place at the end of a marked rainfall episode. For this date, the retrieved SSM was high and exceeded 0.40 $m^3\,m^{-3}$ at the central part of the transect. The end of the 2009 campaign was relatively dry, and the last rainfall events

HESSD
9, 895–936, 2012

(24–26 May) triggered an increase of the retrieved SSM in the central part of transect, only. In 2010 two marked rainfall episodes occurred from 29 April to 14 May and from 6 June to 19 June. At the end of May 2010, more local precipitation events took place in different parts of the transect.

Figure 6 presents the retrieved CAROLS SSM along the Atlantic-Mediterranean transect in contrasting 2009 and 2010 conditions (end of April and end of May), together with the SSM simulated by ISBA-A-gs. At the end of April, the CAROLS SSM values observed in 2009 are systematically higher than the 2010 values. At the end of May, the CAROLS SSM is higher in 2009 close to the Atlantic coast and for the eastern part of the transect, and lower at the central part of the transect. Figure 6 shows that the same SSM differences between 2010 and 2009 dates can be observed for the simulated SSM. Also, the spatial distribution of the CAROLS SSM measurements is in good agreement with that of the modelled SSM. The lowest SSM values are observed in the forested Atlantic part of the transect and close to the Mediterranean coast. Table 2 shows that the spatial correlation between the two datasets is significant (p-value < 0.05) for all the twenty flights, with correlation coefficients ranging from 0.36 to 0.85 and root mean square differences (RMSD) ranging from 0.05 to 0.20 $m^3\,m^{-3}$. On average, RMSD = 0.083 $m^3\,m^{-3}$ and SDD = 0.066 $m^3\,m^{-3}$.

3.2.2 LAI and VOD

The VOD values retrieved from CAROLS Tb range from 0.05 to 0.35. The highest VOD values are found in forested areas, presenting an average VOD value of 0.2. The arable lands are characterised by low VOD values varying between 0.05 and 0.15. Figure 7 shows that the ISBA-A-gs simulated LAI increases sharply in 2009 and in 2010, from the end of April to the end of May, from 0.8 $m^2\,m^{-2}$ in the Les Landes forest to 1.2 $m^2\,m^{-2}$ in the other parts of the transect. In 2010, the airborne campaign lasted 2.5 months and the simulated LAI increases, on average, from about 2 $m^2\,m^{-2}$ in the Les Landes forest, to 2.6 $m^2\,m^{-2}$ in the central agricultural part of the transect, and to 1.8 $m^2\,m^{-2}$ in the eastern Mediterranean part. However, the CAROLS VOD retrievals

HESSD
9, 895–936, 2012

do not show marked changes during these periods. For most grid cells, the temporal variability of the retrieved VOD, either seasonal or interannual, is very low and not significant (Fig. 7).

In spite of the lack of temporal correlation between the CAROLS VOD and the ISBA-A-gs LAI, they present a similar spatial distribution (Fig. 7). The spatial correlation coefficient between the ISBA-A-gs LAI and the CAROLS VOD varies from 0.34 to 0.85 for the nineteen flights presenting a significant correlation. The slope of this relationship changes with time (Fig. 8), decreasing from April to July (Table 3). The comparison of the VOD spatial distribution with the monthly climatology of MODIS-derived LAI confirms this tendency (Fig. 8).

Inverting Eq. (4) for the 19 flights presenting a significant spatial correlation between VWC and VOD, mean values of $b_{\text{high}} = 0.16 \pm 0.03\,\text{m}^2\,\text{kg}^{-1}$ and $b_{\text{low}} = 0.09 \pm 0.07\,\text{m}^2\,\text{kg}^{-1}$ are obtained. The spatial correlation between the CAROLS VOD and the aggregated model-derived VOD is significant for nineteen flights, with correlation coefficients varying from 0.31 to 0.61 (Fig. 8 and Table 2). The mean RMSD and bias values are 0.07 and 0.03, respectively. Figure 9 shows that the spatial distribution of the CAROLS VOD retrievals aggregated at the grid-cell level is consistent with the simulated VOD for high vegetation. From 28 April 2010 to 4 June 2010, the simulated VOD for low vegetation increases significantly and this increase does not appear in the CAROLS VOD retrievals.

3.3 Small-scale spatial heterogeneity of SSM and VOD

In order to assess the local heterogeneity of SSM and VOD, we calculated and analysed the standard deviation (std) of the CAROLS retrievals within each ISBA-A-gs grid cell, using the over-sampling capability of the instrument (see Sect. 2.4). For 83 % of the model's grid cells std(SSM) and std(VOD) present relatively low values: $\text{std(SSM)} \leq 0.05\,\text{m}^3\,\text{m}^{-3}$ and $\text{std(VOD)} \leq 0.05$. High values of std(SSM) and std(VOD) are found for 5 % of the model's grid cells: $\text{std(SSM)} > 0.08\,\text{m}^3\,\text{m}^{-3}$ and

HESSD
9, 895–936, 2012

std(VOD) > 0.08. The grid-cells presenting the highest sub-grid variability are found on the western part of the transect, in the Les Landes forest area. In the central part of the transect they are found close to the Auch city (between Peyrusse and Lahas in Fig. 1), and close to the Garonne river valley. In the eastern part of the transect, they are found in the hilly areas with a high fraction of bare soil and deciduous forests.

4 Discussion

4.1 Causes of mismatch between SSM estimates

The CAROLS SSM retrievals may present significant biases with respect to the in situ SMOSMANIA observations (Table 1 and Fig. 4), and to the ISBA-A-gs simulations (Fig. 6). Part of these differences may be caused by the spatial heterogeneity of SSM, which is not fully represented in any of the SSM estimates considered in this study (Sect. 3.3). Also, as shown by Fig. 10, large scale geographic patterns such as soil texture and vegetation types, may trigger systematic differences in the representation of soil moisture. Along the Atlantic-Mediterranean CAROLS transect, the SSM difference between CAROLS and the ISBA-A-gs model is consistent with the CAROLS SSM departure from the in situ observations. This indicates that the CAROLS SSM retrievals behave differently from the other two SSM estimates. Although the mean bias (over 20 flights) between the CAROLS and ISBA-A-gs SSM is low and equal to $-0.02\,m^3\,m^{-3}$, it presents a high spatial variability with a standard deviation of $0.07\,m^3\,m^{-3}$. The same spatial distribution of the bias is observed for all the flights (not shown). The best agreement between airborne measurements and model simulations is found in the eastern part of the transect with an average bias between these datasets less than $0.01\,m^3\,m^{-3}$. In the Armagnac region at the western part of the transect, between 0.5° W and 1° E, the CAROLS SSM retrievals are constantly lower, on average, of about $-0.06\,m^3\,m^{-3}$. In the central part of the transect, corresponding to the Garonne river valley, between 1° E and 1.5° E, the bias is positive, of about $0.05\,m^3\,m^{-3}$ on average. This area is

HESSD
9, 895–936, 2012

characterised by the highest discrepancy between the CAROLS and ISBA-A-gs SSM estimates, and the maximal difference can reach 0.38 $m^3 m^{-3}$. It must be noted that although a series of filters was applied to the CAROLS dataset in order to mitigate the perturbing factors (see Sects. 2.1.4 and 2.3), the influence on SSM of open waters like river channels or small ponds has not been fully eliminated (Sect. 3.3). Using high resolution Landsat GeoCover Mosaic images, it was checked that areas with individual SSM reaching 0.5 $m^3 m^{-3}$ in Fig. 2 correspond to regions presenting a high density of small water bodies. Also, the lower CAROLS SSM values in the western part of the transect may be the signature of possible unfiltered low-level RFI. Nevertheless, the large scale spatial pattern in the CAROLS/ISBA-A-gs SSM bias (Fig. 10) is more likely explained by the fact that the SSM values, in units of $m^3 m^{-3}$, retrieved from the CAROLS Tb, are affected by shortcoming of the L-MEB inversion process. Indeed, key processes affecting the microwave emission are not represented, such as the topography and its impact on the angular signature of Tb and on the spatial distribution of soil moisture. Also, a number of studies have shown that the impact of vegetation debris and litters is represented with difficulty by L-MEB (Saleh et al., 2006, 2007). The latter factor may affect all the vegetation types, but grasslands and forests tend to favour the formation of a litter. Finally, soil roughness may vary from one vegetation type to another, and also for a given vegetation type. Using Eq. (1) to represent soil roughness for all the transect is probably too simple. The same kind of criticism may apply to the ISBA-A-gs simulations. However, the main factors affecting SSM are accounted for by the model. The maximum SSM and the rate at which SSM varies after a rain, in relation to the root-zone soil moisture value, depend on pedotransfer functions driven by soil characteristics such as soil texture (Noilhan and Lacarrère, 1995). The model uses a map of soil properties and represents, also, the interception of rain by the vegetation. Fig. 10 suggests that high values of either the sand proportion of the soil or the fraction of forest, tend to match the areas where the CAROLS SSM values are lower than the simulated ones. This may denote the limit of using the single Eq. (1) to represent soil roughness over all the CAROLS transect. Pardé et al. (2011) shown that the accuracy

HESSD
9, 895–936, 2012

of the soil moisture retrieval from CAROLS Tb observations can be improved, up to $0.053\,m^3\,m^{-3}$, through local soil roughness calibration.

4.2 From VOD to VWC

The b parameter for low vegetation obtained in this study ($b_{low} = 0.09 \pm 0.07\,m^2\,kg^{-1}$) is close to the value $0.12 \pm 0.03\,m^2\,kg^{-1}$ that was found to be representative of most agricultural crops by Wigneron et al. (2007). On the other hand, the estimated b parameter for high vegetation ($b_{high} = 0.16 \pm 0.03\,m^2\,kg^{-1}$) is lower than the value of $0.33\,m^2\,kg^{-1}$ reported in Pellarin et al. (2003), or than the range of values (0.26 to $0.34\,m^2\,kg^{-1}$) used to retrieve VOD of high vegetation from SMOS measurements (Kerr et al., 2007). Moreover, Fig. 8 and Table 3 show that the CAROLS VOD retrievals correlate with both LAI observations and aggregated LAI simulations, and that the VOD sensitivity to LAI (either observed or modelled) tends to decrease along the growing season. The model simulations permit to investigate the sub-grid variability of the b parameter and to distinguish the temporal evolution of b_{low} and b_{high} (Fig. 11). While the flight to flight variability of b_{high} is small, the b_{low} values present a significant seasonal trend (Fig. 11) and ranges from values close to $0.15\,m^2\,kg^{-1}$ in April, to values close to $0.05\,m^2\,kg^{-1}$ at summertime. The b_{low} trend is significant and equal to $-0.0012\,m^2\,kg^{-1}\,day^{-1}$. The decrease of b_{low} during the vegetation period compensates for the rise in VWC, and this may explain the absence of significant temporal variability in the CAROLS VOD retrievals (Figs. 7 and 9). These figures are consistent with the L-band b values given by Wigneron et al. (1996) for a wheat field, ranging from $0.125\,m^2\,kg^{-1}$ for green vegetation at the start of the growing season, to $0.040\,m^2\,kg^{-1}$ at the end of June. Wigneron et al. (1996) attributed this trend to changes in the leaf microwave properties, from the growing phase to the senescence.

HESSD
9, 895–936, 2012

5 Conclusions

In this paper, we have presented an analysis of the data acquired during the CAROLS flights that took place in Southwestern France, between the Atlantic and the Mediterranean coasts, in April–May 2009 and in April–July 2010. These data were acquired to validate the retrieval algorithm used for the L2 SMOS SSM processing, and to investigate the accuracy of L-band soil moisture sensing over a large area presenting variable soil and vegetation conditions.

The microwave L-band Tb were affected by RFI. A post-processing filtering based on the TbH vs. TbV analysis at nadir and slant looking angles, permitted to improve the SSM and VOD datasets. After applying this filtering, a relatively good agreement between the airborne SSM and in situ SSM observations was achieved, with a correlation coefficient ranging from 0.51 to 0.82, and RMSD and SDD values ranging from 0.04 to 0.21 $m^3\,m^{-3}$, and from 0.04 to 0.14 $m^3\,m^{-3}$, respectively. Better scores were obtained with the ASCAT SSM product at the same in situ stations (Albergel et al., 2009), as well as with SSM values derived from the SMOS Tb through regression equations derived from the CAROLS observations (Albergel et al., 2011). On the other hand, the spatial variability of the airborne SSM and VOD retrievals was consistent with the ISBA-A-gs simulations. For all the flights, the spatial correlation between ISBA-A-gs and CAROLS SSM was significant (p-value < 0.05) with r and RMSD values varying between 0.36 and 0.85 and between 0.05 and 0.20 $m^3\,m^{-3}$, respectively.

The sub-grid variability of CAROLS SSM and VOD within ISBA-A-gs grid cells was relatively low. Along the Atlantic-Mediterranean transect, 83 % of ISBA grid cells presented a spatial variability of CAROLS SSM retrievals lower than 0.05 $m^3\,m^{-3}$, a figure comparable with the accuracy acceptable for remotely sensed SSM estimates (Walker and Houser, 2004). It was found that small water bodies (100–300 m in length) had a significant impact on the CAROLS measurements.

HESSD
9, 895–936, 2012

Finally, it was found that the *b* parameter for low vegetation may present a seasonal variation and this effect should be investigated further as it is currently not accounted for in L-band microwave emission models.

The results of this work show the potential of the L-band to monitor SSM over large regions. On the other hand, the L-MEB optimisation technique depends on hypotheses, particularly on soil roughness, and this may affect the quality of the SSM retrievals. Also, it is shown that deriving VWC estimates from VOD retrievals is difficult, because forest and herbaceous vegetation present contrasting VWC responses to VOD. In the case of herbaceous vegetation, the VOD response to LAI varies with time, with a decreasing sensitivity from springtime to summertime.

Acknowledgements. This work was supported by the STAE (Sciences et Technologies pour l'Aéronautique et l'Espace) foundation, in the framework of the CYMENT project, as well as by Centre National d'Etudes Spatiales (CNES) and Météo-France. The CAROLS project was funded by the "Programme Terre Océan Surface Continentales et Atmosphère" (TOSCA, CNES). The ATR-42 aircraft was operated by the SAFIRE UMS 2859. S. Lafont was supported by the GEOLAND2 project, cofunded by European Commission within the GMES initiative in FP7.

The publication of this article is financed by CNRS-INSU.

HESSD
9, 895–936, 2012

References

Albergel, C., Rüdiger, C., Pellarin, T., Calvet, J.-C., Fritz, N., Froissard, F., Suquia, D., Petitpa, A., Piguet, B., and Martin, E.: From near-surface to root-zone soil moisture using an exponential filter: an assessment of the method based on in-situ observations and model simulations, Hydrol. Earth Syst. Sci., 12, 1323–1337, doi:10.5194/hess-12-1323-2008, 2008.

Albergel, C., Rüdiger, C., Carrer, D., Calvet, J.-C., Fritz, N., Naeimi, V., Bartalis, Z., and Hasenauer, S.: An evaluation of ASCAT surface soil moisture products with in-situ observations in Southwestern France, Hydrol. Earth Syst. Sci., 13, 115–124, doi:10.5194/hess-13-115-2009, 2009.

Albergel, C., Calvet, J.-C., de Rosnay, P., Balsamo, G., Wagner, W., Hasenauer, S., Naeimi, V., Martin, E., Bazile, E., Bouyssel, F., and Mahfouf, J.-F.: Cross-evaluation of modelled and remotely sensed surface soil moisture with in situ data in southwestern France, Hydrol. Earth Syst. Sci., 14, 2177–2191, doi:10.5194/hess-14-2177-2010, 2010.

Albergel, C., Zakharova, E., Calvet, J.-C., Zribi, M., Pardé, M., Wigneron, J.-P., Novello, N., Kerr, Y., Mialon, A., and Fritz, N.: A first assessment of the SMOS data in Southwestern France using in situ and airborne soil moisture estimates: the CAROLS airborne campaign, Remote Sens. Environ., 115, 2718–2728, doi:10.1016/j.rse.2011.06.012, 2011.

Bircher, S., Balling, J. E., Skou, N., and Kerr, Y.: Validation of SMOS brightness temperatures during the HOBE airborne campaign, Western Denmark, IEEE Trans. Geosci. Remote Sens., submitted, 2012.

Brut, A., Rüdiger, C., Lafont, S., Roujean, J.-L., Calvet, J.-C., Jarlan, L., Gibelin, A.-L., Albergel, C., Le Moigne, P., Soussana, J.-F., Klumpp, K., Guyon, D., Wigneron, J.-P., and Ceschia, E.: Modelling LAI at a regional scale with ISBA-A-gs: comparison with satellite-derived LAI over southwestern France, Biogeosciences, 6, 1389–1404, doi:10.5194/bg-6-1389-2009, 2009.

Calvet, J.-C.: Investigating soil and atmospheric plant water stress using physiological and micrometeorological data, Agr. Forest Meteorol., 103, 229–247, 2000.

Calvet, J.-C. and Soussana, J.-F.: Modelling CO_2-enrichment effects using an interactive vegetation SVAT scheme, Agr. Forest Meteorol., 108, 129–152, 2001.

Calvet, J.-C., Noilhan, J., Roujean, J.-L., Bessemoulin, P., Cabelguenne, M., Olioso, A., and Wigneron, J.-P.: An interactive vegetation SVAT model tested against data from six contrasting sites, Agr. Forest Meteorol., 92, 73–95, 1998.

HESSD
9, 895–936, 2012

Calvet, J.-C., Rivalland, V., Picon-Cochard, C., and Guehl, J.-M.: Modelling forest transpiration and CO_2 fluxes – response to soil moisture stress, Agr. Forest Meteorol., 124, 143–156, doi:10.1016/j.agrformet.2004.01.007, 2004.

Calvet, J.-C., Fritz, N., Froissard, F., Suquia, D., Petitpa, A., and Piguet, B.: In-situ soil moisture observations for the CAL/VAL of SMOS: the SMOSMANIA network, International Geoscience and Remote Sensing Symposium, IGARSS, Barcelona, Spain, 1196–1199, doi:10.1109/IGARSS.2007.4423019, 23–28 July 2007.

Calvet, J.-C., Wigneron, J.-P., Walker, J., Karbou, F., Chanzy, A., and Albergel, C.: Sensitivity of passive microwave observations to soil moisture and vegetation water content: L-band to W-band, IEEE Trans. Geosci. Remote Sens., 49, 1190–1199, doi:10.1109/TGRS.2010.2050488, 2011.

Cano, A., Saleh, K., Wigneron, J. P., Antolín, C., Ballinge, J., Kerr, Y., Kruszewski, A., Millán-Scheiding, C., Søbjærge, S., Skoue, N., and López-Baeza E.: The SMOS Mediterranean Ecosystem L-Band characterisation EXperiment (MELBEX-I) over natural shrubs, Remote Sens. Environ., 114, 844–853, 2010.

Chanzy, A., Schmugge, T. J., Calvet, J.-C., Kerr, Y., van Oevelen, P., Grosjean, O., and Wang, J. R.: Airborne microwave radiometry on a semi-arid area during HAPEX-Sahel, J. Hydrol., 188–189, 285–309, 1997.

Davidson, A., Wang, Sh., and Wilmshurst, J.: Remote sensing of grassland–shrubland vegetation water content in the shortwave domain, Int. J. Appl. Earth Obs. Geoinf., 8, 225–236, 2006.

De Rosnay, P., Calvet, J.-C., Kerr, Y., Wigneron, J. P., Lemaıtre, F., Escorihuela, M. J., Munoz Sabater, J., Saleh, K., Barrie, J., Coret, L., Cherel, G., Dedieu, G., Durbe, R., Fritz, N., Froissard, F., Kruszewski, A., Lavenu, F., Suquia, D., and Waldteufel, P.: SMOSREX: A long term field campaign experiment for soil moisture and land surface processes remote sensing, Remote Sens. Environ., 102, 377–389, 2006.

De Rosnay, P., Gruhier, C., Timouk, F., Baup, F., Mougin, E., Hiernaux, P., Kergoat, L., and LeDantec, V.: Multi-scale soil moisture measurements at the Gourma meso-scale site in Mali, J. Hydrol., 375, 241–252, 2009.

Dobson, M. C., Ulaby, F. T., Hallikainen, M. T., and El-Rayes, M. A.: Microwave dielectric behavior of wet soil – Part II: dielectric mixing models, IEEE Trans. Geosci. Remote Sens., GE-23, 35–46, 1985.

HESSD
9, 895–936, 2012

Draper, C. S., Walker, J. P., Steinle, P. J., de Jeu, R., and Holmes, T.: An evaluation of AMSR–E derived soil moisture over Australia, Remote Sens. Environ., 113, 703–710, 2007.

Drusch, M., Wood, E. F., Gao, H., and Thiele, A.: Soil moisture retrieval during the Southern Great Plains Hydrologic Experiment 1999: A comparison between experimental remote sensing data and operational products, Water Resour. Res., 40, W02504, doi:10.1029/2003WR002441, 2004.

Durand, Y., Brun, E., Merindol, L., Guyomarc'h, G., Lesaffre, B., and Martin, E.: A meteorological estimation of relevant parameters for snow models, Ann. Glaciol., 18, 65–71, 1993.

Faroux, S., Roujean, J.-L., Kaptué, A., and Masson, V.: La base de données de paramètres de surface ECOCLIMAP-II sur l'Europe, Note de centre du Groupe de Météorologie à Moyenne Echelle, 86, Météo-France, CNRM, Toulouse, France, 120 pp., 2009.

Grant, J. P., Saleh-Contell, K., Wigneron, J. P., Guglielmetti, M., Kerr, Y., Schwank, M., Skou, N., and Van de Griend, A. A.: Calibration of the L-MEB model over a coniferous and a deciduous forest, IEEE Trans. Geosci. Remote Sens., 46, 808–818, 2008.

Gruhier, C., de Rosnay, P., Hasenauer, S., Holmes, T., de Jeu, R., Kerr, Y., Mougin, E., Njoku, E., Timouk, F., Wagner, W., and Zribi, M.: Soil moisture active and passive microwave products: intercomparison and evaluation over a Sahelian site, Hydrol. Earth Syst. Sci., 14, 141–156, doi:10.5194/hess-14-141-2010, 2010.

Guglielmetti, M., Schwank, M., Matzler, C., Oberdorster, C., Vanderborght, J., and Fluhler, H.: FOSMEX: forest soil moisture experiments with microwave radiometry, IEEE Trans. Geosci. Remote Sens., 46, 727–735, 2008.

Jackson, T., Hawley, M. E., Shuie, J., O'Neill, P. E., Owe, M., Delnore, S. V., and Lawrence, R. W.: Assessment of preplanting soil moisture using airborne microwave sensors, Hydrologic Applications of Space Technology, Proceedings of the Cocoa Beach Workshop, Florida, August 1985, IAHS Publ., 160, 111–118, 1986.

Jones, O., Jones, L., Kimball, J., and McDonald, K.: Satellite passive microwave remote sensing for monitoring global land surface phenology, Remote Sens. Environ., 115, 1102–1114, 2011

Kerr, Y., Waldteufel, P., Wigneron, J.-P., Martinuzzi, J.-M., Font, J., and Berger, M.: Soil moisture retrieval from space: the soil moisture and ocean salinity (SMOS) mission, IEEE Trans. Geosci. Remote Sens., 39, 1729–1736, 2001.

HESSD
9, 895–936, 2012

Knyazikhin, Y., Marshak, J. V., Diner, D. J., Verstraete, M., and Gobron, N.: Estimation of vegetation canopy leaf area index and fraction of absorbed photosynthetically active radiation from atmosphere-corrected MISR data, J. Geophys. Res., 103, 32239–32257, 1998.
Kochendorfer, J. P. and Ramírez, J. A.: Modeling the monthly mean soil-water balance with a statistical-dynamical ecohydrology model as coupled to a two-component canopy model, Hydrol. Earth Syst. Sci., 14, 2099–2120, doi:10.5194/hess-14-2099-2010, 2010.
Masson, V., Champeaux, J.-L., Chauvin, F., Meriguet, C., and Lacaze, R.: A global database of land surface parameters at 1-km resolution in meteorological and climate models, J. Climate, 16, 1261–1282, 2003.
Myneni, R., Knyazikhin, Y., Glassy, J., Votava, V., and Shabanov, N.: FPAR, LAI (ESDT: MOD15A2) 8-day Composite NASA MODIS Land Algorithm, User's Guide, 1–17, 2003.
Noilhan, J. and Lacarrère, P.: GCM gridscale evaporation from mesoscale modelling, J. Climate, 8, 206–223, 1995.
Panceira, R., Walker, J. P., Kalma, J. D., Kim, E. J., Hacker J. M., Merlin, O., Berger, M., and Skou, N.: The NAFE'05/CoSMOS data set: toward SMOS soil moisture retrieval, downscaling and assimilation, IEEE Trans. Geosci. Remote Sens., 46, 736–746, 2008.
Pardé, M., Zribi, M., Fanise, P., and Dechambre, M.: Analysis of RFI issue using the CAROLS L-Band experiment, IEEE Trans. Geosci. Remote Sens., 49, 1063–1070, 2011a.
Pardé, M., Zribi, M., Wigneron, J. P., Dechambre, M., Fanise, P., Kerr, Y., Crapeau, M., Saleh, K., Calvet, J.-C., Albergel, C., Mialon, A., and Novello, N.: Soil moisture estimations based on airborne CAROLS L-band microwave data, Remote Sens., 3, 2591–2604, doi:10.3390/rs3122591, 2011b.
Parrens, M., Zakharova, E., Lafont, S., Calvet, J.-C., Kerr, Y., Wagner, W., and Wigneron, J.-P.: Comparing soil moisture retrievals from SMOS and ASCAT over France, Hydrol. Earth Syst. Sci., submitted, 2012.
Pellarin, T., Wigneron, J. P., Calvet, J.-C., and Waldteufel, P.: Global soil moisture retrieval from a synthetic L-band brightness temperature data set, J. Geophys. Res., 108, 4364, 2003.
Pellarin, T., Calvet, J.-C., and Wagner, W.: Evaluation of ERS scatterometer soil moisture products over a half-degree region in Southwestern France, Geophys. Res. Lett., 33, L17401, doi:10.1029/2006GL027231, 2006.
Penuelas, J., Filella, I., Biel, C., Serrano, L., and Save, R.: The reflectance at the 950–970 mm region as an indicator of plant water status, Int. J. Remote Sens., 14, 1887–1905, 1993.

HESSD
9, 895–936, 2012

Rüdiger, C., Calvet, J.-C., Gruhier, C., Holmes, T., De Jeu, R., and Wagner, W.: An intercomparison of ERS-Scat and AMSR-E soil moisture observations with model simulations over France, J. Hydrometeorol., 10, 431–447, doi:10.1175/2008JHM997.1, 2009.

Saleh, K., Wigneron, J. P., Calvet, J.-C., Lopez-Baeza, E., Ferrazzoli, P., Berger, M., Wursteisen, P., Simmonds, L., and Miller, J.: The EuroSTARRS airborne campaign in support of the SMOS mission: first results over land surfaces, Int. J. Remote Sens., 25, 177–194, 2004.

Saleh, K., Wigneron, J.-P., de Rosnay, P., Calvet, J.-C., and Kerr, Y.: Semi-empirical regressions at L-band applied to surface soil moisture retrieval over grass, Remote Sens. Environ., 101, 415–426, 2006.

Saleh, K., Wigneron, J.-P., Waldteufel, P., de Rosnay, P., Schwank, M., Calvet, J.-C., and Kerr, Y. H.: Estimates of surface soil moisture under grass covers using L-band radiometry, Remote Sens. Environ., 109, 42–53, 2007.

Saleh, K., Kerr, Y. H., Richaume, P., Escorihuela, M. J., Panciera, R., Delwart, S., Boulet, G., Maisongrande, P., Walker, J. P., Wursteisen, P., and Wigneron, J. P.: Soil moisture retrievals at L-band using a two-step inversion approach (COSMOS/NAFE'05 Experiment), Remote Sens. Environ., 113, 1304–1312, 2009.

Schmugge, T., Jackson, T. J., Kustas, W. P., and Wang, J. R.: Passive microwave remote sensing of soil moisture: results from HAPEX, FIFE and MONSOON 90, J. Photogram. Remote Sens., 47, 127–143, 1992.

Su, Z., Timmermans, W. J., van der Tol, C., Dost, R., Bianchi, R., Gómez, J. A., House, A., Hajnsek, I., Menenti, M., Magliulo, V., Esposito, M., Haarbrink, R., Bosveld, F., Rothe, R., Baltink, H. K., Vekerdy, Z., Sobrino, J. A., Timmermans, J., van Laake, P., Salama, S., van der Kwast, H., Claassen, E., Stolk, A., Jia, L., Moors, E., Hartogensis, O., and Gillespie, A.: EAGLE 2006 – Multi-purpose, multi-angle and multi-sensor in-situ and airborne campaigns over grassland and forest, Hydrol. Earth Syst. Sci., 13, 833–845, doi:10.5194/hess-13-833-2009, 2009.

Wagner, W., Lemoine, G., and Rott, H.: A method of estimating soil moisture from ERS scatterometer and soil data, Remote Sens. Environ., 70, 191–207, 1999a.

Wagner, W., Noll, J., Borgeaud, M., and Rott, H.: Monitoring soil moisture over the Canadian prairies with the ERS scatterometer, IEEE Trans. Geosci. Remote Sens., 37, 206–216, 1999b.

HESSD
9, 895–936, 2012

Walker, J. P. and Houser, P. R.: Requirements of global near surface soil moisture satellite mission: accuracy, repeat time and spatial resolution, Adv. Water Resour., 27, 785–801, 2004.
Wang, J. R. and Choudhury, B. J.: Remote sensing of soil moisture content over bare field at 1.4 GHz frequency, J. Geophys. Res., 86, 5277–5282, 1981.
Wang, S.: Dynamics of surface albedo of a boreal forest and its simulation, Ecol. Model., 183, 477–494, 2005.
Wigneron, J.-P., Chanzy, A., Calvet, J.-C., and Bruguier, N.: A simple algorithm to retrieve soil moisture and vegetation biomass using passive microwave measurements over crop fields, Remote Sens. Environ., 5, 331–341, 1995.
Wigneron, J.-P., Calvet, J.-C., and Kerr, Y.: Monitoring water interception by crop fields from passive microwave observations, Agr. Forest Meteorol., 80, 177–194, 1996.
Wigneron, J.-P., Chanzy, A., Calvet, J.-C., Olioso, A., and Kerr, Y.: Modeling approaches to assimilating L band passive microwave observations over land surfaces, J. Geophys. Res., 107, 14 pp., doi:10.1029/2001JD000958, 2002.
Wigneron, J.-P., Kerr, Y., Waldteufel, P., Saleh, K., Escorihuela, M.-J., Richaume, P., Ferrazzoli, P., de Rosnay, P., Gurney, R., Calvet, J.-C., Grant, J. P., Guglielmetti, M., Hornbuckle, B., Mätzler, C., Pellarin, T. and Schwankh, M.: L-band microwave emission of the biosphere (L-MEB) model: description and calibration against experimental data sets over crop fields, Remote Sens. Environ., 107, 639–655, 2007.
Wigneron, J.-P., Chanzy, A., de Rosnay, P., Rüdiger, C., and Calvet, J.-C.: Estimating the effective soil temperature at L-band as a function of soil properties, IEEE Trans. Geosci. Remote Sens., 46, 797–801, 2008.
Zhao, D., Kuenzer, C., Fu, C., and Wagner, W.: Evaluation of the ERS scatterometer-derived soil water index to monitor water availability and precipitation distribution at three different scales in China, J. Hydrometeorol., 9, 549–562, 2008.
Zribi, M., Pardé, M., Boutin, J., Fanise, P., Hauser, D., Dechambre, M., Kerr, Y., Leduc-Leballeur, M., Skou, M., Søbjærg, S. S., Albergel, C., Calvet, J.-C., Wigneron, J.-P., Lopez-Baeza, E., Ruis, A., and Tenerelli, J.: CAROLS: a new airborne L-band radiometer for ocean surface and land observations, Sensors, 11, 719–742, 2011.

HESSD
9, 895–936, 2012

Table 1. Comparison of SSM time series for (from left to right) SMOSMANIA vs. CAROLS, CAROLS vs. ISBA-A-gs, ISBA-A-gs vs. SMOSMANIA. Correlation coefficient (r), p-value, RMSD, bias (SMOSMANIA minus CAROLS, CAROLS minus ISBA-A-gs, ISBA-A-gs minus SMOSMANIA, respectively) and the standard deviation of differences (SDD) for the pooled 2009 and 2010 CAROLS flights. NS (non significant), *, **, *** stand for p-values greater than 0.05, between 0.05 and 0.01, between 0.01 and 0.001, and below 0.001, respectively.

Station	r	p-value	RMSD ($m^3\,m^{-3}$)	Mean bias ($m^3\,m^{-3}$)	SDD ($m^3\,m^{-3}$)	N_{obs}
SBR	0.36/0.54/0.69	NS/*/***	0.069/0.064/0.069	−0.024/−0.034/0.058	0.065/0.056/0.037	20
URG	0.56/0.50/0.64	*/*/**	0.212/0.077/0.168	0.195/−0.046/−0.149	0.085/0.063/0.080	20
CRD	0.66/0.55/0.68	**/*/***	0.102/0.069/0.092	−0.080/−0.005/0.085	0.063/0.069/0.036	20
PRG	0.23/0.58/0.67	NS/**/**	0.175/0.157/0.067	−0.012/−0.028/0.040	0.175/0.157/0.055	17
CDM	0.41/0.61/0.61	NS/**/**	0.134/0.090/0.085	0.088/−0.018/−0.070	0.101/0.090/0.050	17
LHS	0.62/0.73/0.59	**/***/**	0.108/0.101/0.064	0.030/−0.009/−0.021	0.105/0.101/0.062	20
SVN	0.51/0.46/0.58	*/*/**	0.212/0.213/0.068	−0.159/0.154/0.005	0.141/0.150/0.068	20
MNT	0.82/0.63/0.64	***/**/**	0.121/0.067/0.150	0.113/0.032/−0.144	0.044/0.060/0.044	17
SFL	0.67/0.74/0.53	**/***/*	0.073/0.066/0.074	−0.017/−0.018/0.029	0.071/0.065/0.069	17
MTM	0.80/0.72/0.54	***/**/*	0.066/0.064/0.039	0.038/−0.031/−0.012	0.054/0.057/0.038	17
LZC	–	–	–	–	–	2
NBN	0.67/0.60/0.66	**/*/**	0.039/0.044/0.043	−0.006/−0.020/0.023	0.039/0.040/0.036	17
AVERAGE	0.57/0.61/0.62	–	0.119/0.097/0.084	0.015/−0.002/−0.014	0.086/0.083/0.052	–

HESSD
9, 895–936, 2012

Table 2. Spatial correlation coefficient (R), p-value, RMSD and SDD ($m^3\,m^{-3}$ for SSM) and number of grid cells taken for score calculation (N_{obs}) between ISBA-A-gs and CAROLS SSM and VOD for 20 flights in 2009 and 2010. *, **, ***, **** stand for p-values between 0.05 and 0.01, between 0.01 and 0.001, between 0.001 and 0.0001 and below 0.0001, respectively. Note that, 22 ISBA-A-gs grid cells presented successful VOD retrievals on 26 June 2010, only. The average significant score values are indicated.

Date	SSM				VOD				N_{obs}
	R	p-value	RMSD ($m^3\,m^{-3}$)	SDD ($m^3\,m^{-3}$)	R	p-value	RMSD (–)	SDD (–)	
28 Apr 2009	0.37	**	0.084	0.083	0.57	****	0.056	0.055	67
15 May 2009	0.61	****	0.098	0.073	0.48	****	0.079	0.053	68
18 May 2009	0.61	***	0.066	0.065	0.57	***	0.063	0.058	40
20 May 2009	0.56	**	0.056	0.052	0.55	**	0.080	0.064	33
26 May 2009	0.37	*	0.092	0.067	0.48	***	0.077	0.066	48
27 May 2009	0.57	****	0.070	0.063	0.49	****	0.075	0.058	67
15 Apr 2010	0.41	**	0.077	0.067	0.56	****	0.052	0.051	68
28 Apr 2010	0.36	**	0.059	0.050	0.61	****	0.055	0.055	68
3 May 2010	0.38	*	0.197	0.137	0.01	NS	0.218	0.126	60
9 May 2010	0.61	****	0.088	0.068	0.43	***	0.081	0.081	66
21 May 2010	0.70	****	0.061	0.059	0.38	***	0.064	0.060	68
26 May 2010	0.85	****	0.074	0.062	0.32	*	0.082	0.080	57
31 May 2010	0.43	***	0.084	0.076	0.51	****	0.077	0.052	71
4 Jun 2010	0.74	****	0.061	0.042	0.61	****	0.083	0.048	66
8 Jun 2010	0.52	***	0.101	0.063	0.18	NS	0.120	0.094	70
13 Jun 2010	0.80	****	0.088	0.079	0.37	**	0.074	0.055	73
18 Jun 2010	0.65	****	0.086	0.085	0.31	**	0.089	0.066	69
22 Jun 2010	0.78	****	0.106	0.060	0.48	****	0.066	0.056	76
26 Jun 2010	0.70	****	0.066	0.028	–0.17	NS	0.154	0.037	62/22
1 Jul 2010	0.80	****	0.049	0.040	0.57	****	0.082	0.046	65
Average	0.59	–	0.083	0.066	0.49	–	0.073	0.059	–

HESSD
9, 895–936, 2012

Table 3. Spatial correlation coefficient (R), p-value, RMSD, and the slopes of the regression lines (Fig. 8) between ISBA-A-gs/MODIS derived LAI and the CAROLS VOD. ***, **** stand for p-values between 0.001 and 0.0001 and below 0.0001, respectively.

Date	R	p-value	RMSD	Slope
		ISBA-A-gs LAI		
15 Apr 2010	0.48	****	1.48	0.096
4 Jun 2010	0.48	****	3.44	0.039
1 Jul 2010	0.44	***	4.03	0.037
		MODIS LAI		
15 Apr 2010	0.20	NS	1.23	0.115
4 Jun 2010	0.57	****	1.59	0.081
1 Jul 2010	0.73	****	1.86	0.077

HESSD
9, 895–936, 2012

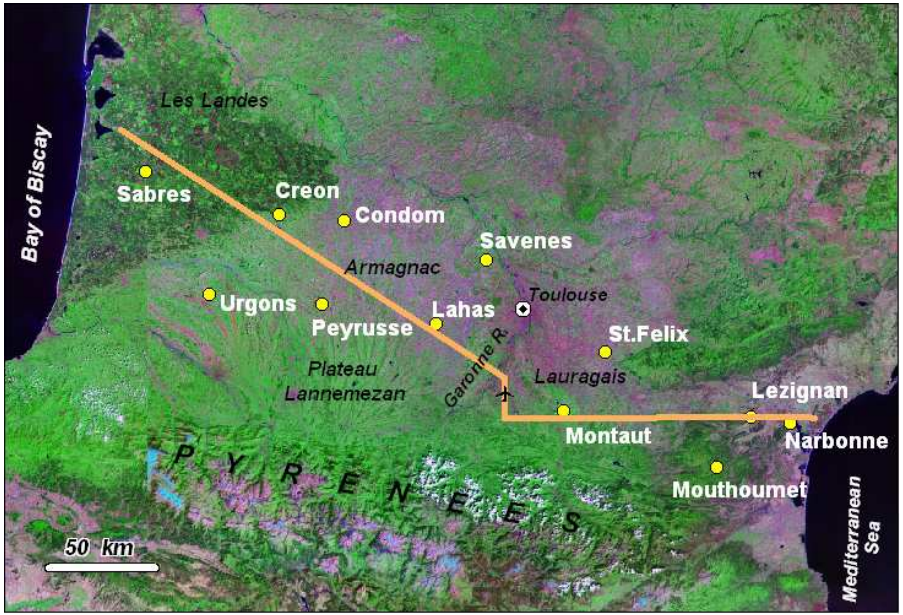

Fig. 1. Atlantic-Mediterranean transect and location of SMOSMANIA stations (background is a Landsat GeoCover Mosaics).

HESSD
9, 895–936, 2012

Spatial and temporal variability of biophysical variables in SW France

E. Zakharova et al.

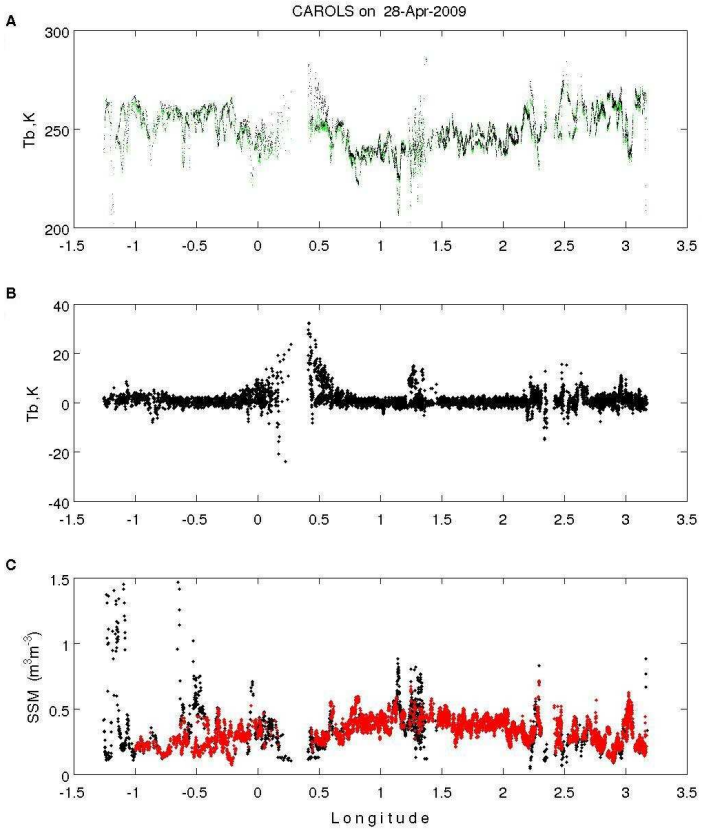

Fig. 2. Spatial variability of **(A)** CAROLS TbH (green) and TbV (black) at nadir, **(B)** CAROLS brightness temperature difference (TbV-TbH) at nadir, and **(C)** CAROLS surface soil moisture, for 28 April 2009. Red dots represent the SSM data after the post processing filtering.

HESSD
9, 895–936, 2012

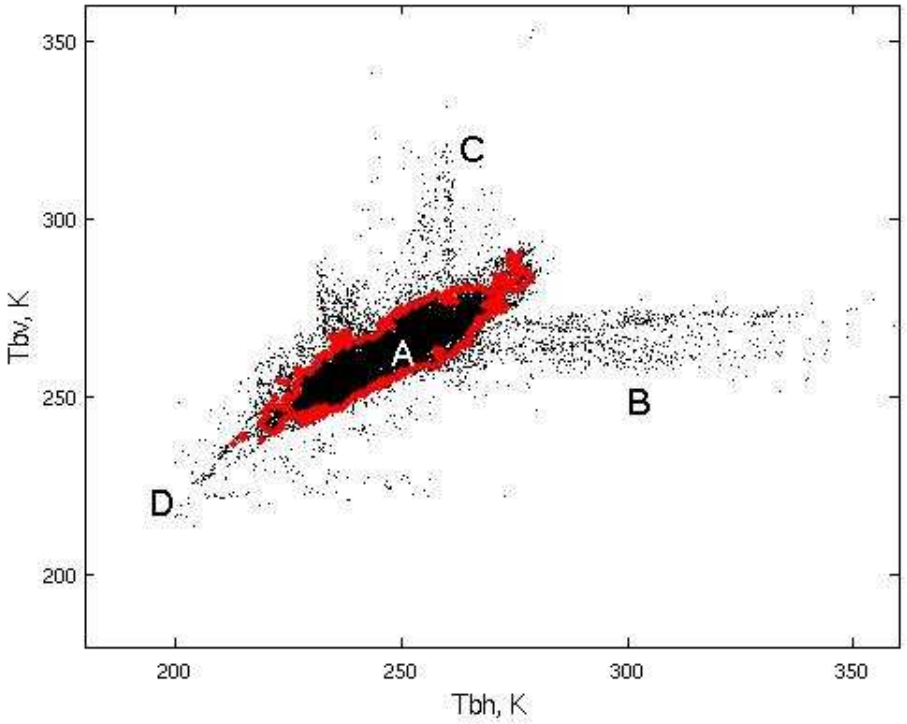

Fig. 3. Side-looking antenna TbV vs. TbH for the six CAROLS flights in 2009. The measurements outside of the red contour were removed from the analysis. See the explanation for the letters in Sect. 2.1.4.

HESSD
9, 895–936, 2012

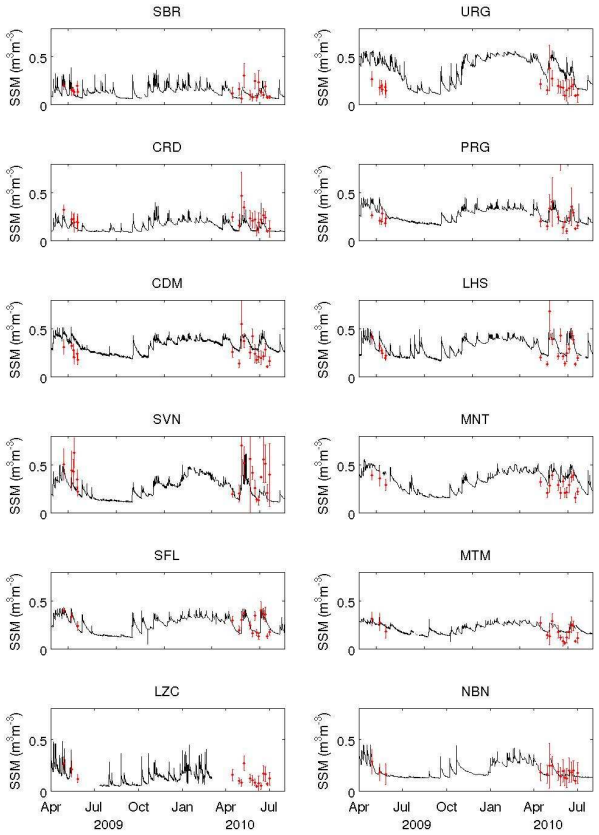

Fig. 4. Temporal variability of the SSM measured by the SMOSMANIA stations (black line) and of the CAROLS SSM (red dots with std error bars): SBR – Sabres, URG – Urgons, CRD – Créon d'Armagnac, PRG – Peyrusse Grande, CDM – Condom, LHS – Lahas, SVN – Savenes, MNT – Montaut, SFL – Saint-Félix de Lauragais, MTM – Mouthoumet, LZC – Lézignan-Corbières, NBN – Narbonne.

HESSD
9, 895–936, 2012

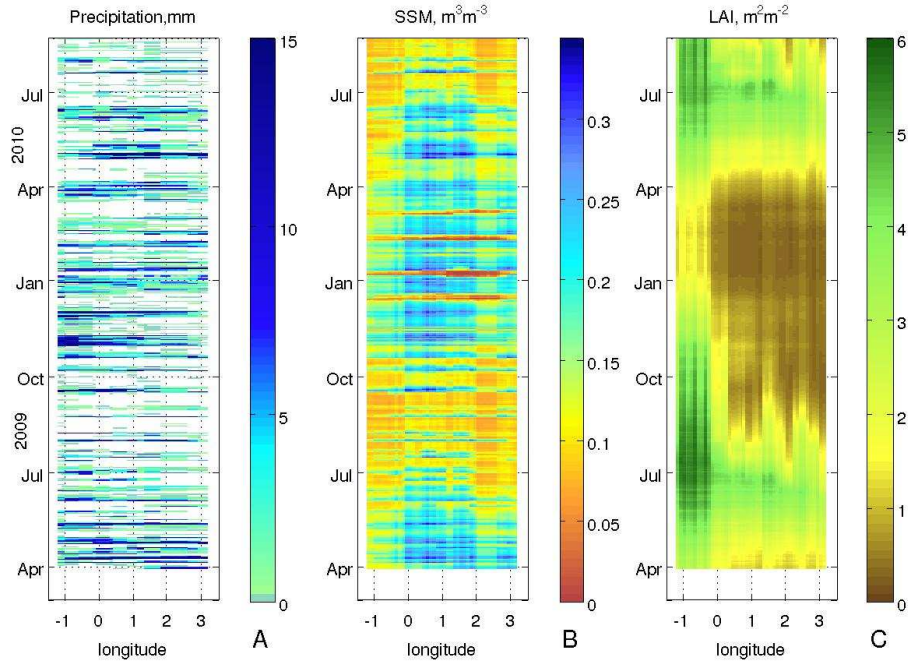

Fig. 5. Spatial and temporal variability of **(A)** precipitation (SAFRAN reanalysis), **(B)** ISBA-A-gs surface soil moisture and **(C)** ISBA-A-gs LAI, during (from bottom to top) the 2009–2010 period, over (from left to right) the CAROLS Atlantic-Mediterranean transect.

HESSD
9, 895–936, 2012

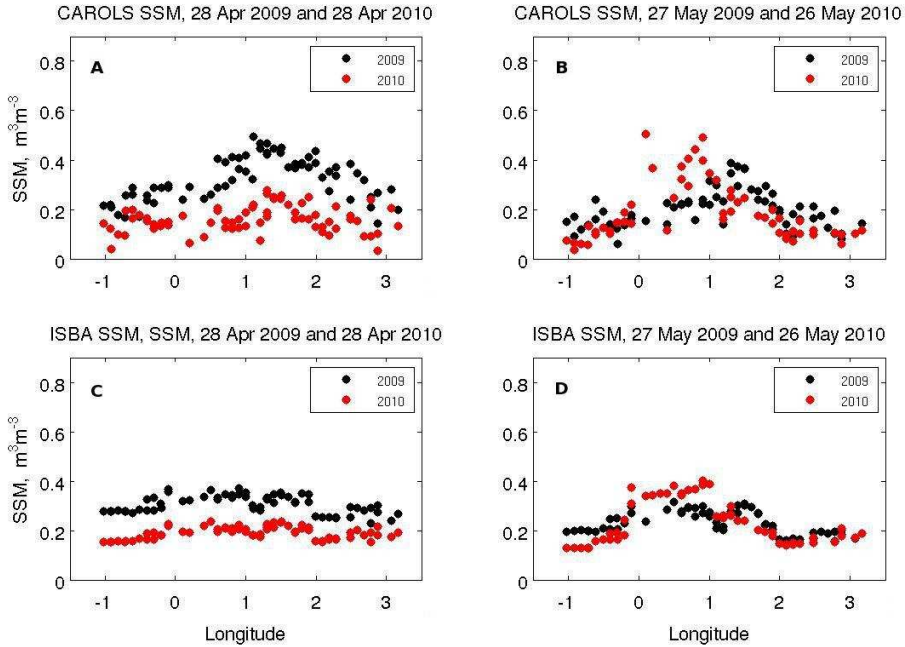

Fig. 6. Along flight interannual variability of the surface soil moisture from **(A, B)** CAROLS retrievals and from **(C, D)** ISBA-A-gs simulations, at **(A, C)** the end of April, and **(B, D)** the end of May.

HESSD
9, 895–936, 2012

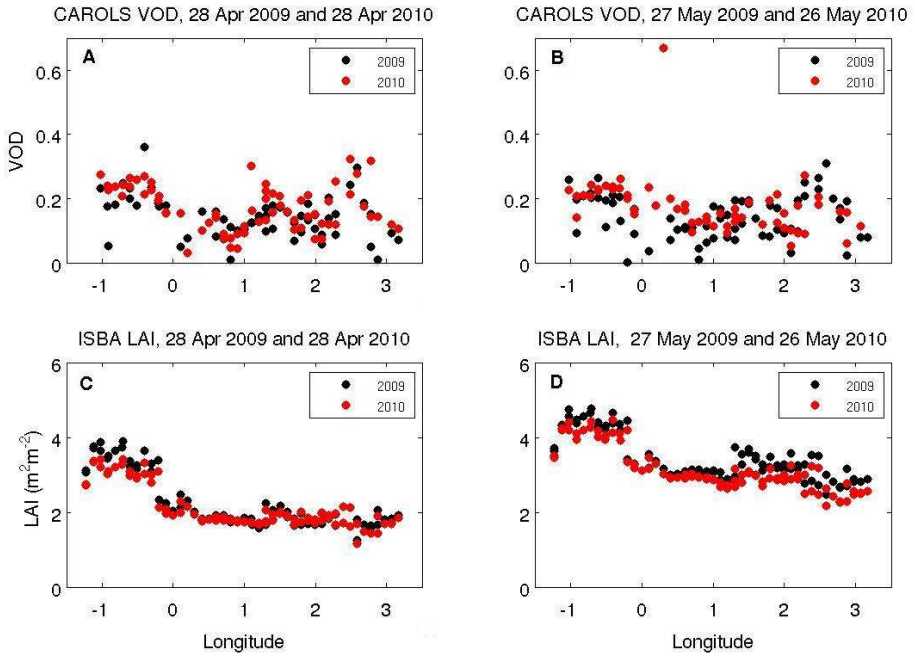

Fig. 7. Along flight interannual variability of **(A, B)** the vegetation optical thickness (VOD) retrieved from CAROLS Tb and of **(C, D)** the ISBA-A-gs LAI simulations, at **(A, C)** the end of April, and **(B, D)** the end of May.

HESSD
9, 895–936, 2012

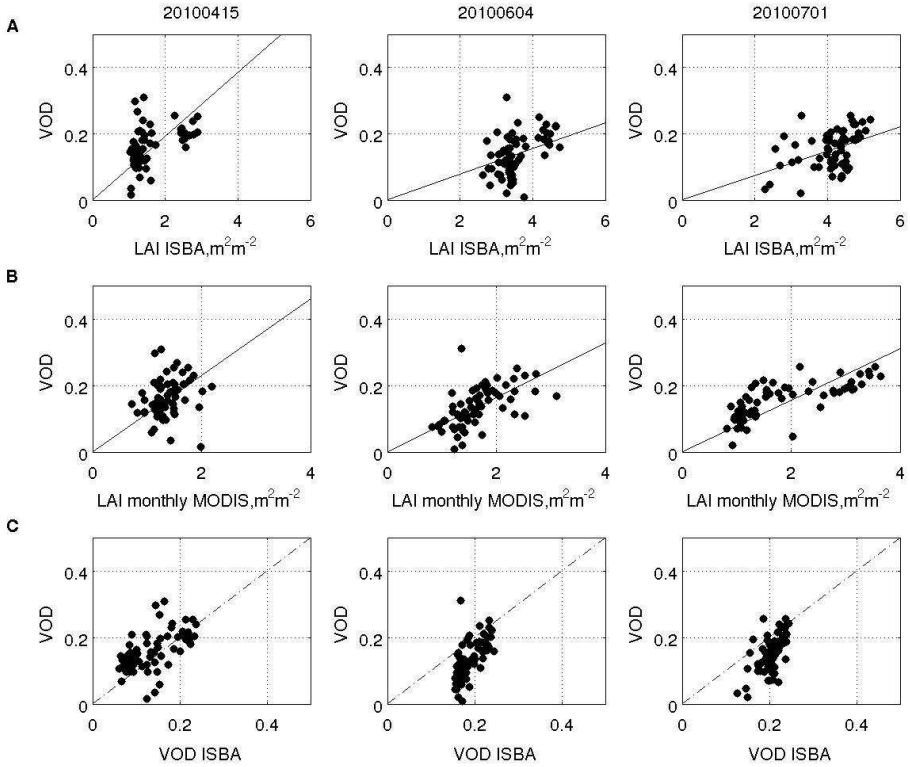

Fig. 8. Spatial correlation between the CAROLS VOD and **(A)** the ISBA-A-gs LAI, **(B)** the MODIS LAI, and **(C)** the VOD estimated from the ISBA-A-gs LAI and the forest fraction from ECOCLIMAP II using the same *b* parameter 0.09 for three dates in 2010: from left to right, 15 April, 4 June, 1 July. The solid lines on plots A and B represent linear regression lines with forced zero intercept.

HESSD
9, 895–936, 2012

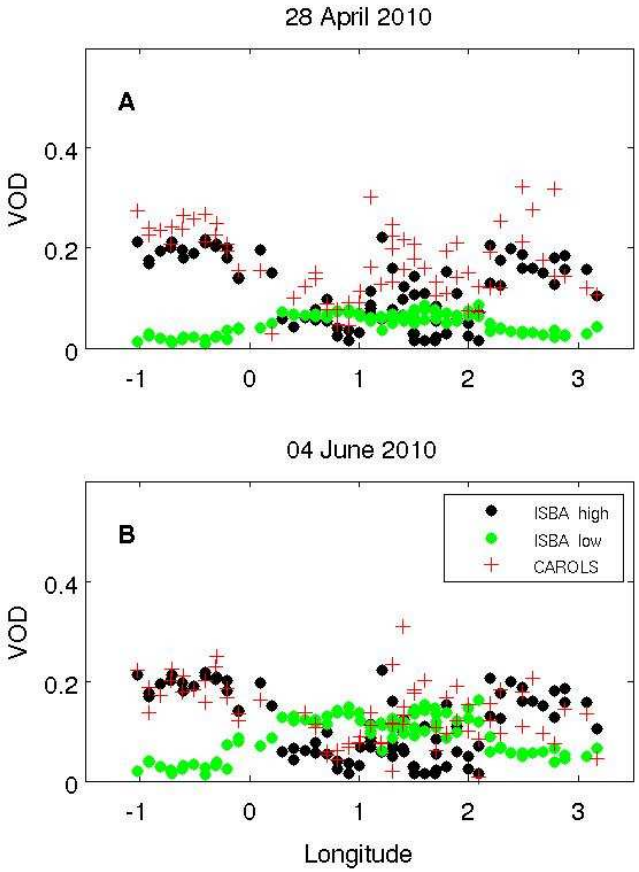

Fig. 9. Along track variability of the CAROLS VOD and the VOD estimated using the ISBA-A-gs LAI of low vegetation, and the forest fraction from ECOCLIMAP II and *b* parameter = 0.09 for low vegetation and 0.16 for high vegetation, for **(A)** 28 April 2010 and **(B)** 4 June 2010.

HESSD
9, 895–936, 2012

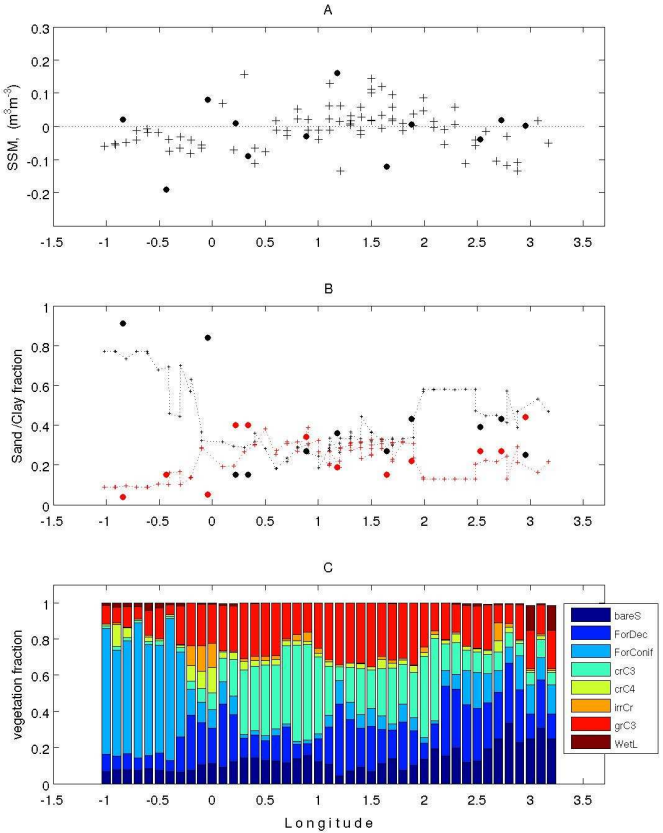

Fig. 10. Spatial variability **(A)** of the CAROLS minus ISBA-A-gs (crosses) and CAROLS minus SMOSMANIA (dots) bias averaged for twenty flights; **(B)** of the sand (black) and clay (red) fraction used for ISBA-A-gs simulations (line) and CAROLS retrievals (dots); **(C)** of the vegetation fraction from ECOCLIMAP-II.

HESSD
9, 895–936, 2012

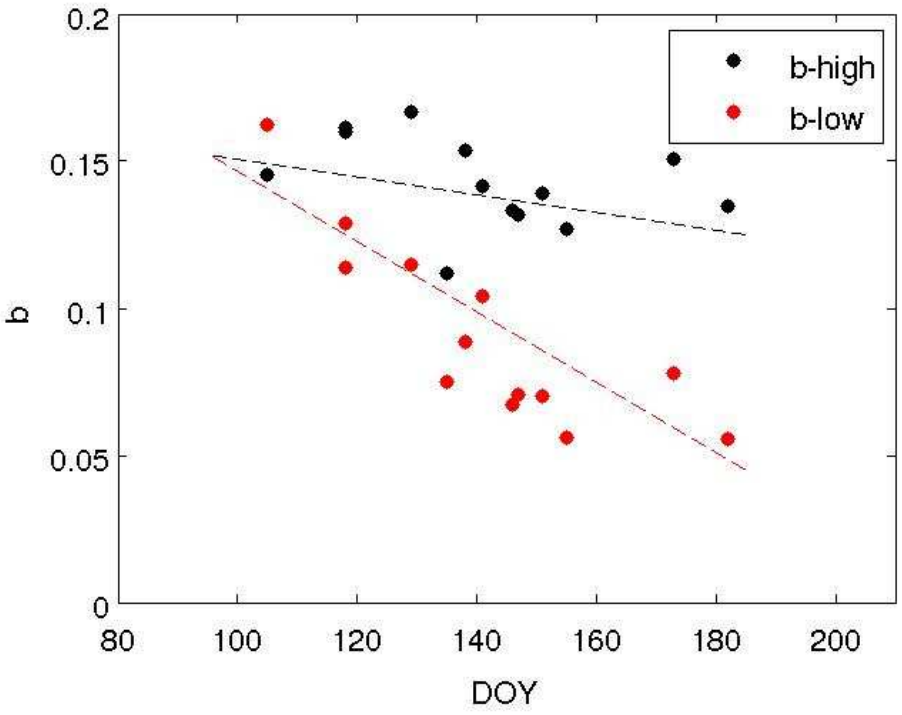

Fig. 11. Temporal variation of the b parameter (in units of $m^2\,kg^{-1}$) for high and low vegetation. For b_{high} the correlation is insignificant with $r = -0.37$; for b_{low} the correlation is significant (p-value = 0.0003 and $r = -0.85$); the trend in b_{low} is significant at the 0.1 % level and equal to $-0.0012\,m^2\,kg^{-1}\,day^{-1}$.

HESSD
9, 895–936, 2012